pubs.acs.org/Biomac

Article

Atomic Level Interactions and Suprastructural Configuration of Plant Cell Wall Polymers in Dialkylimidazolium Ionic Liquids

Aparna Annamraju, Kalavathy Rajan, Xiaobing Zuo, Brian K. Long, Sai Venkatesh Pingali, Thomas J. Elder, and Nicole Labbé*

Cite This: https://doi.org/10.1021/acs.biomac.3c00047

Read Online

ACCESS | Metrics & More | Article Recommendations | Supporting Information

ABSTRACT: Ionic liquids (ILs) have been widely investigated for the pretreatment and deconstruction of lignocellulosic feedstocks. However, the modes of interaction between IL-anions and cations, and plant cell wall polymers, namely, cellulose, hemicellulose, and lignin, as well as the resulting ultrastructural changes are still unclear. In this study, we investigated the atomic level and suprastructural interactions of microcrystalline cellulose, birchwood xylan, and organosolv lignin with 1,3-dialkylimidazolium ILs having varying sizes of carboxylate anions. Analysis by ^{13}C NMR spectroscopy indicated that cellulose and lignin exhibited stronger hydrogen bonding with acetate ions than with formate ions, as evidenced by greater chemical shift changes. Small-angle X-ray scattering analysis showed that while both cellulose and xylan adopted a single-stranded conformation in acetate-ILs, twice as many acetate ions were bound to one anhydroglucose unit than to an anhydroxylose unit. We also determined that a minimum of seven representative carbohydrate units must interact with an anion for that IL to effectively dissolve cellulose or xylan. Lignin is associated as groups of four polymer molecules in formate-ILs and dispersed as single molecules in acetate-ILs, which indicates that it is highly soluble in the latter. In summary, our study demonstrated that 1,3-dialkylimidazolium acetates displayed stronger binding interactions with cellulose and lignin, as compared to formates, and thus have superior potential to fractionate these polymers from lignocellulosic feedstocks.

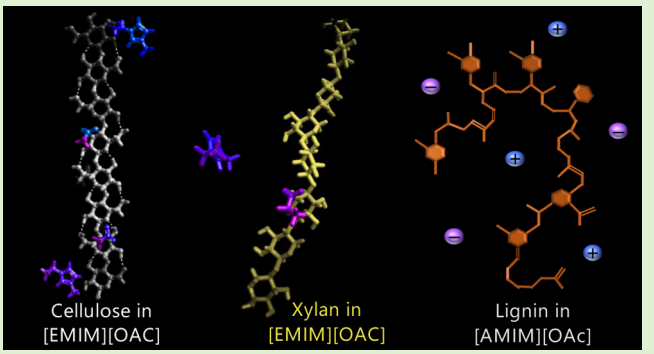

INTRODUCTION

Lignocellulosic feedstocks, such as agricultural residues, forest biomass, and dedicated bioenergy crops, are abundant and renewable resources composed of three main polymers, *i.e.*, cellulose, hemicellulose, and lignin.[1] Although there have been extensive attempts in the past three decades to use these feedstocks for fuel and value-added products, progress is still hindered by the inherent recalcitrance of lignocellulosic biomass.[1] Physicochemical treatments have been developed to reduce this recalcitrance but were mostly optimized for the isolation and conversion of cellulose.[2] Thus, these biomass conversion routes left behind hemicellulose and lignin, which are potential low-cost feedstocks for the production of bio-based chemicals and materials.[3,4] Recently, targeted valorization efforts have ensured better utilization of xylan and lignin as raw material in fuels, resins, films, composites, and other applications.[4,5] However, the effective fractionation of the three most abundant plant cell wall polymers is still a challenge.

One key step in the isolation and utilization of cellulose, hemicellulose, and lignin is designing an efficient solvent system that fractionates these biopolymers without causing significant damage to their native structure and generating undesired products. Solvent systems, such as *N*-methylmorpholine-*N*-oxide (NMMO),[6,7] dimethyl sulfoxide/tetrabutylammonium fluoride,[8] and butanol/acetic acid,[9] have been reported to dissolve one or more of the lignocellulosic components, but they suffer from drawbacks such as low fractionation efficiency, noxious odor, toxicity, and/or volatility. Ionic liquids (ILs), on the other hand, exhibit superior solvation capability, low vapor pressure, and high thermal stability, making them an attractive choice for green processing technologies.[10] These low-melting salts feature an organic cation and an organic or inorganic anion, and their physicochemical properties, such as viscosity and polarity, are customizable by changing the cation/anion combination.[10] ILs containing a chloride anion, *i.e.*, 1-butyl-3-methylimidazolium chloride ([BMIM][Cl]), have been demonstrated to dissolve up to 25% (w/w) of cellulose.[11] Similarly, imidazolium-based

Received: January 12, 2023
Revised: March 2, 2023

ILs containing a methanesulfonate anion could dissolve about 45% (w/w) of milled wood lignin,[12] whereas [BMIM][Cl] could dissolve up to 19% (w/w) of bamboo hemicellulose.[13] Although these ILs have been identified as potential solvents to fractionate lignocellulosic biomass, the underlying mechanism for some IL-ion pairs such as chloride and methanesulfonate to outperform others like bromide, phosphate, and acetate is not well understood. Hence, a comprehensive investigation of the interactions between IL-ion pairs and cellulose, hemicellulose, and lignin is warranted to help select ILs for efficient fractionation of lignocellulosic biomass.

In previous studies, atomic and molecular level interactions between IL-ion pairs and lignocellulosic model systems like microcrystalline cellulose, cellobiose, xylan, guaiacol glyceryl ether, and milled wood lignin were probed using experimental (nuclear magnetic resonance (NMR) spectroscopy) and theoretical (density functional theory or DFT) techniques. ^{1}H, ^{13}C, and $^{35/37}$Cl NMR analysis of [BMIM][Cl],[14] 1-ethyl-3-methylimidazolium acetate ([EMIM][OAc]), 1-ethyl-3-methylimidazolium tetrafluoroborate,[15,16] and 1-allyl-3-methylimidazolium carboxylates,[17] at different temperatures and solute concentrations, showed that the chloride and acetate anions underwent a significant change in nuclei relaxation time as well as chemical shifts in the presence of model cellulose compounds. NMR analysis of IL-ion pair interactions showed that although dissolution temperature and cation structure were important, hydrogen bonding between IL-anion and arabinoxylan was the key determinant for solubilization.[18] Theoretical DFT calculations showed that the binding energy between xylan and IL-ion pairs was 20 kcal mol^{-1} higher than with cellobiose.[19] Similarly, DFT modeling of polyphenols showed that hydrogen bonding and $\pi-\pi$ stacking with IL-cation may be essential for lignin dissolution.[20] 2D NMR analysis of lignin model compounds dissolved in dialkylimidazolium ILs provided inconclusive evidence of hydrogen bonding between lignin hydroxyl groups and the C2 proton of [BMIM] cation.[21] It is thus crucial to obtain empirical evidence of IL-ion pair interactions with all three biopolymers, *i.e.*, cellulose, hemicellulose, and lignin, to design efficient IL-based solvent systems.

In addition to probing atomic level interactions, suprastructural evaluations using small-angle X-ray scattering (SAXS) can help to elucidate details such as biopolymer conformation and morphology in different ILs. For example, microcrystalline cellulose was shown to assume a rigid rod-like conformation in [EMIM][OAc] at length scales smaller than the persistent length.[22] However, in a subsequent study, microcrystalline cellulose was reported to adopt a flexible conformation in [BMIM][Cl].[23] This difference in conformation was assigned to the chloride anion's superior ability to disrupt not only the inter- but also the intramolecular hydrogen bonds in cellulose. In another study, where microcrystalline cellulose was dissolved in deuterated [EMIM][OAc], it was determined that [EMIM][OAc] permeated between individual cellulose fibers, bound tightly to the cellulose strands, thereby peeling away individual fibrils, and ultimately brought about cellulose dissolution.[24] Similarly, SAXS analysis could be used to determine the IL-ion pair binding with cellulose, hemicellulose, and lignin, such that we can quantitatively evaluate biopolymer dissolution in different ILs.

The objective of this study was to elucidate the atomic level interactions and suprastructural conformation of cellulose, hemicellulose, and lignin in select ILs that differ in their anion/cation pairs. We used 1,3-dialkylimidazolium ILs, containing formate and acetate anions, to dissolve representative plant cell wall polymers and evaluate their differential interactions by NMR and SAXS. Most of the previous reports have used either acetate or chloride anions as test systems but not formates.[25] Formate-ILs have lower room temperature viscosity than acetate-ILs and could dissolve a higher weight percentage of cellulose, thus exhibiting the potential for wider utility in plant biomass processing.[26] We used SAXS to determine the suprastructural conformation of not only cellulose but also xylan and lignin. Thus, this study provides new insights into the interactions of 1,3-dialkylimidazolium ILs with plant cell wall polymers such that it will aid in the selection of IL-ion pairs for optimal lignocellulosic biomass fractionation.

EXPERIMENTAL SECTION

Materials. The four ILs used in this study, namely, 1-ethyl-3-methylimidazolium formate ([EMIM][HCOO]), 1-ethyl-3-methylimidazolium acetate ([EMIM][OAc]), 1-allyl-3-methylimidazolium formate ([AMIM][HCOO]), and 1-allyl-3-methylimidazolium acetate ([AMIM][OAc]), were purchased from IoLiTec GmbH (Tuscaloosa, AL). The carbon atom notations for the cations and anions are provided in Figure 1.

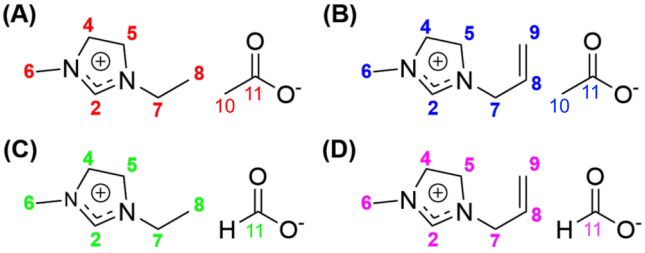

Figure 1. Chemical structures and carbon atom notations for (A) [EMIM][OAc], (B) [AMIM][OAc], (C) [EMIM][HCOO], and (D) [AMIM][HCOO].

The moisture content of [EMIM][HCOO], [EMIM][OAc], [AMIM][HCOO], and [AMIM][OAc] was determined to be 10.9 ± 1.4, 8.9 ± 0.7, 6.1 ± 0.4, and 4.6 ± 0.5%, respectively, by heating a representative IL sample of 2 to 5 mg in a Pyris 1 thermogravimetric analyzer (TGA, PerkinElmer, Shelton, CT) at 105 °C for approximately 15 min or until constant weight (under air).

Avicel PH-101 microcrystalline cellulose (DP = 350) was purchased from Alfa Aesar (Tewksbury, MA), and birchwood xylan (≥90% xylose) was purchased from Sigma-Aldrich (St. Louis, MO), and used as received. Lignin was produced from hybrid poplar wood chips using an organosolv fractionation process at the Center for Renewable Carbon, University of Tennessee, Knoxville.[27] Briefly, 650 g of wood chips were fractionated using a solvent mixture of 50:34:16 (w/w/w) water, ethanol, and methyl isobutyl ketone, containing 0.05 M sulfuric acid as catalyst, at 140 °C for 120 min. The purity of the isolated organosolv lignin, based on acid-soluble lignin and Klason lignin estimation, was 94.6 ± 0.2%, and its molecular weight (M_w) was 3743 g/mol, with a dispersity of 1.2.[27] The moisture content of Avicel cellulose, birchwood xylan, and organosolv lignin, determined gravimetrically, was 2.9 ± 0.1, 12.5 ± 0.4, and 3.6 ± 0.1%, respectively. Dimethyl sulfoxide-d_6 (DMSO-d_6, 99.9%) containing tetramethyl silane (0.03%, v/v) was purchased from Cambridge Isotope Laboratories Inc. (Tewksbury, MA).

Preparation of Biopolymer-IL Solutions. The biopolymer-IL solutions were prepared by dissolving 10% (w/w) of the cellulose, xylan, and lignin in each IL at 80 °C. First, 2 g of ILs were weighed out in a vial and heated at 100 °C for 10 min to remove excess moisture. The temperature was then reduced to 80 °C, and the

https://doi.org/10.1021/acs.biomac.3c00047
Biomacromolecules XXXX, XXX, XXX−XXX

biopolymer was added in 20 mg increments until the target mass of 200 mg was reached. The dissolution of the biopolymers was confirmed by placing an aliquot under a bright-field optical microscope (20× magnification); the absence of visible aggregate particles was assumed to indicate complete dissolution. The moisture content at 80 °C of the neat ILs and biopolymer-IL solutions, determined using the TGA (to replicate the NMR testing conditions), are listed in the Supporting Information (Table S1); it was determined that the moisture content for all samples ranged between 0.5 and 3.0% (w/w).

^{13}C NMR Analysis of Biopolymer-IL Solutions. Samples for ^{13}C NMR analysis were prepared by mixing 575 μL of the above-mentioned biopolymer-IL solution and 125 μL of DMSO-d_6. A control containing 575 μL of neat IL and 125 μL of DMSO-d_6 was also prepared. DMSO-d_6 has been shown to aid in the dissociation of IL-cation and anion without altering or participating in interactions with cell wall biopolymers like cellulose.[28] Our preliminary experiments determined that a minimum amount of 125 μL of DMSO-d_6 was needed to provide a lock frequency.

NMR spectra were recorded on a Bruker 400 MHz spectrometer (Billerica, MA) at 353 K (80 °C). Both DMSO-d_6 and tetramethyl silane were used as internal references. The change in chemical shift for each carbon was calculated by subtracting the chemical shift of neat IL from that of biopolymer-IL solutions. The data were processed (baseline correction and chemical shift assignment) using Mnova software, version 14.2 (Mestrelab Research, A Coruña, Spain). Each experiment was repeated at least three times. A one-way ANOVA was performed to determine any significant differences in the chemical shift changes; the significance level was set at $\alpha = 0.05$. All statistical analyses were conducted using IBM SPSS Statistics for Windows, version 26.0 (IBM Corp., Armonk, NY).

SAXS and WAXS Experiments. Small-angle and wide-angle X-ray scattering (SAXS and WAXS) experiments were conducted at the 12-ID-B beamline of Advanced Photon Source (Argonne National Laboratory, Lemont, IL). All measurements were carried out at room temperature. A 2% (w/w) biopolymer concentration was employed to ensure that individual molecular features were delineated and the differences in IL-anion/cation association with plant polymer components could be discerned. Solutions of 2% (w/w) cellulose, xylan, and lignin were prepared in select ILs, injected into a 2 mm diameter capillary tube, sealed with epoxy, and then used for SAXS analysis. The X-ray wavelength was 0.9322 Å, and a PILATUS (Dectris) detector was used as the area detector. The irradiation time was 10 s (1 s irradiation repeated 10 times). The observed X-ray scattering intensities were normalized to absolute intensity using glassy carbon (a secondary standard sample for intensity calibration).[29] The scattering intensity, $I(Q)$, of cellulose, xylan, and lignin in the different ILs was obtained after subtracting the scaled scattering intensity of the corresponding neat IL. The scaling factor of the neat IL for each sample was determined by comparing the WAXS data of the biopolymer-IL solution and the neat IL, where only the IL background scattering signal was dominant.

SAXS data for cellulose in ILs were analyzed using the model fitting approach implemented in the Irena package in Igor Pro (WaveMetrics, Inc., Portland, OR) software.[30] Cellulose was modeled as cylinders with a Gaussian distribution of radii, which is expressed as follows

$$I(Q) = I_o\overline{P(Q)}S(Q) \tag{1}$$

where I_o is the intensity scalar, which is given by the equation below

$$I_o = \frac{\phi}{V_{poly}}(\Delta\rho)^2 \tag{2}$$

where (ϕ) accounts for the cylinder particle concentration with a polydisperse volume and $\Delta\rho$, calculated as ($\rho_{cylinder} - \rho_{solvent}$), is the contrast between cellulose and solvent. $\rho_{cylinder}$ and $\rho_{solvent}$ are the scattering length densities of the cylinder particles (cellulose) and the solvent, respectively. V_{poly}, the volume of polydisperse cylinders using the second moment, is given as $V_{poly} = \pi r^2 L(1 + p^2)$, where r and L are the cylinder's radius and length, respectively. Polydispersity of the cylinder, $p = \sigma/r_{avg}$, is the ratio of the width of Gaussian distribution to its center. The form factor of a radially polydisperse cylinder, modeled as Gaussian distribution, is expressed as

$$\overline{P(Q)} = \int_0^{\pi/2} (G(r)F^2(q, \alpha)\sin\alpha \, d\alpha) \tag{3}$$

where F is the form factor of a cylinder and $G(r)$ is the radial Gaussian distribution function expressed as

$$F(q, \alpha) = 2V_{cyl}J_0(qH\cos\alpha)\frac{J_1(qr\sin\alpha)}{(qr\sin\alpha)} \tag{4}$$

$$G(r) = \frac{1}{\sigma\sqrt{2\pi}}\int_0^x \exp\left[-\frac{1}{2\sigma^2}(r - r_{avg})^2\right]dr \tag{5}$$

In eq 4, $J_0(x) = \sin(x)/x$ is the zeroth order Bessel function, α is the angle between the cylinder axis and the scattering vector, and H equals half the length of the cylinder (=2L). For our current analysis, a polydisperse function in cylindrical fit was set to the limit of a monodisperse cylinder, and no inter-particle correlation was used, *i.e.*, $S(Q) = 1$.

SAXS data of xylan in IL solution were fit to a single power-law function (Irena package[30]) for the Q-range of 0.03 to 0.15 Å^{-1}

$$I(Q) = (AQ)^{-P} + I_{bkg} \tag{6}$$

where A is the length scale factor, I_{bkg} is the background intensity of neat IL, and P is the power-law exponent.

The lignin SAXS data in IL solution were analyzed using a one- and two-level Unified fit,[31] which is a combination of Guinier and power-law functions as shown below

$$I(Q) = \sum_{i-1}^{N}\left\{G_i\exp\left[-\frac{q^2R_g^2}{3}\right] + B_i\left[\frac{erf(qR_{g,i}/\sqrt{6})^3}{q}\right]^{P_i}\right\} + I_{bkg} \tag{7}$$

where $N = 1$ for single-level fit and $N = 2$ for two-level fit, G_i is the Guinier prefactor of the ith level, B_i is the prefactor of the power-law function of the ith level, P_i is the power-law exponent of the ith level, $R_{g,i}$ is the radius of gyration of the ith level, and I_{bkg} is the background intensity of neat IL. Irrespective of the number of levels used in the fit, the level-1 component on the Unified fit is most important for detailing the lignin particle's structural characteristics. $R_{g,1}$ provides a measure of the shape-independent particle size, and exponent P_1 is a measure of the polymer conformation in the particle (or bulk chain conformation).

RESULTS AND DISCUSSION

Atomic Interactions of Biopolymers with IL-Cations and Anions. We first investigated the atomic level interactions between IL-ion pairs and representative plant cell wall polymers, *i.e.*, cellulose, xylan, and lignin, using ^{13}C NMR spectroscopy. We selected ILs composed of [EMIM] and [AMIM] cations, and [HCOO] and [OAc] anions, based on previous lignocellulose solubility reports.[25,26] The ^{13}C NMR spectra of these neat ILs and the corresponding 10% (w/w) solutions of cellulose, xylan, and lignin are included in the Supporting Information (Figures S1−S16). As seen in Figure 2, carbon atoms in both IL-ion pairs, namely, C2, C4, C5, and C10, exhibited a negative, *i.e.*, upfield chemical shift ($\Delta\delta$) of approximately −0.22, −0.02, −0.06, and −0.12 ppm, respectively, in the presence of 10% (w/w) cellulose. This is indicative of an increase in electron density around these atoms and a subsequent increase in shielding. On the other hand, atoms such as C6, C7, and C11 exhibited a consistent positive, *i.e.*, downfield chemical shift ($\Delta\delta$) of approximately 0.09, 0.07,

https://doi.org/10.1021/acs.biomac.3c00047
Biomacromolecules XXXX, XXX, XXX−XXX

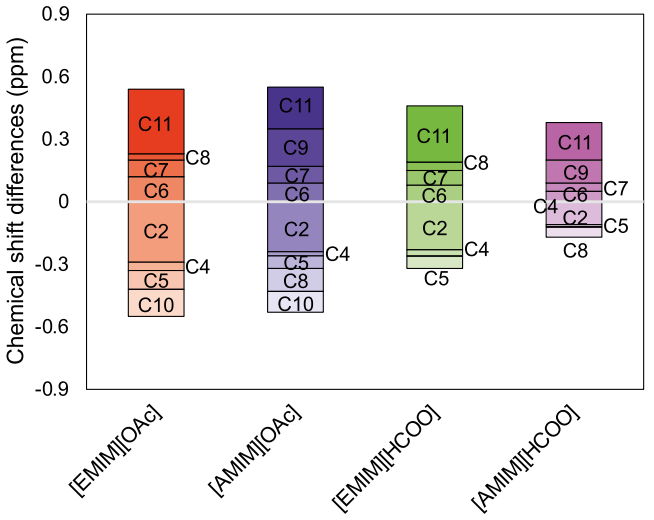

Figure 2. Changes in chemical shift values ($\delta_{(\text{cellulose+IL})} - \delta_{(\text{IL})}$) of all carbon atoms in [EMIM][OAc], [AMIM][OAc], [EMIM][HCOO], and [AMIM][HCOO], each containing 10% (w/w) of cellulose, measured by ^{13}C NMR spectroscopy at 80 °C.

and 0.24 ppm, respectively (Figure 2), indicating a decrease in electron density around these atoms in the presence of cellulose and a subsequent deshielding. Similar results were observed for all IL-ion pair carbons in the presence of xylan and lignin (Figure 3A,B). The corresponding chemical shift change data are provided in Tables S2−S4.

The marked increase in shielding at C2 in the presence of cellulose is in agreement with the prior studies investigating interactions with [EMIM][OAc],[15,16] as well as studies using arabinoxylan or milled wood lignin as model systems.[12,18] The shielding effect may be attributed to the polarity-induced charge difference, such as when the C2 atom interacts with the hydroxyl groups of cellulose, xylan, or lignin.[15−17,25] On average, the increase in shielding was pronounced for the acetate set of ILs when compared to formate-ILs, specifically in the presence of cellulose and lignin (Figures 2 and 3). Between the three biopolymers, the increase in shielding of C2 was the most intense in the presence of cellulose, followed by xylan and then lignin. Other imidazolium ring carbons, namely, C4 and C5 also exhibited an upfield chemical shift and an increase in shielding in the presence of all three biopolymers but at a lower magnitude than C2. The lower magnitude of change is likely due to the lower acidity of C4 and C5 protons and their diminished ability to form hydrogen bonds.[15,16,32]

The C6 atom in the methyl group, as well as the C7 and C9 atoms in the ethyl and allyl side chains, exhibited a downfield chemical shift in the presence of all three biopolymers. However, the trend for C8 atom was different in that when possessing an ethyl side chain, C8 exhibited a downfield chemical shift, whereas when substituted with an allyl side chain, it exhibited an upfield chemical shift. The upfield chemical shift of C8 in [AMIM] ILs could be due to hydrogen bonding between their protons and the hydroxyl oxygen of cellulose, xylan, or lignin. This in turn would have led to electron withdrawal from the C9 atom of [AMIM] cations, causing a deshielding effect, as seen in Figures 2 and 3. A previous study had proposed that the C6 and C7 atoms of [AMIM] cations interacted less with the hydroxyl groups of cellulose than the corresponding C8 or C9 atoms because of their proximity to the nitrogen atoms of the imidazolium ring.[17] Similarly, in our study, the C6 ($\Delta\delta \sim 0.06$ ppm) and C7 ($\Delta\delta \sim 0.06$ ppm) atoms of [AMIM] exhibited lower magnitude of chemical shift changes than C8 ($\Delta\delta \sim -0.10$ ppm) and C9 ($\Delta\delta \sim 0.14$ ppm) atoms in the presence of cellulose, xylan, and lignin (Figures 2 and 3).

In the case of IL-anions, a downfield chemical shift was observed for the carbonyl C11 atom (Figures 2 and 3) that could be explained based on hydrogen bonding interaction between IL's oxygen and the hydroxyl proton in cellulose, xylan, and lignin resulting in a significant decrease in electron density. Since the acetate anion is a stronger conjugate base (pK_a 4.75) than the formate anion (pK_a 3.75),[33] the C11 atom of acetate anion could form a stronger hydrogen bond with all three biopolymers. Previous research has expounded on the significance of IL-anions in bringing about the dissolution of cellulose,[11] but such reports are lacking for xylan and lignin. In this current study, when comparing the absolute changes in chemical shifts of C11, the largest change was observed for

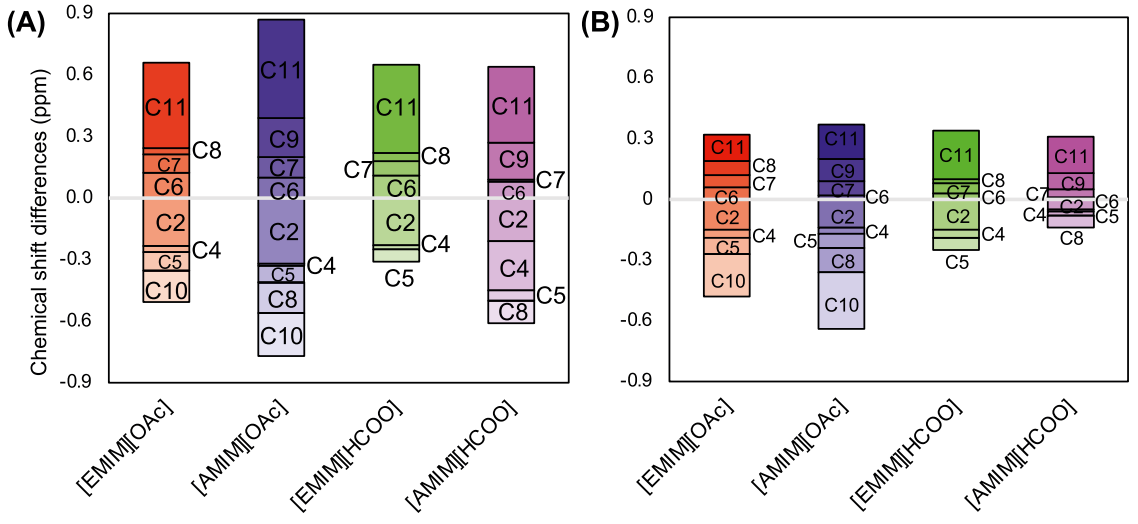

Figure 3. Changes in chemical shift values ($\delta_{(\text{xylan/lignin+IL})} - \delta_{(\text{IL})}$) of all IL carbon atoms in the presence of (A) 10% (w/w) birchwood xylan and (B) 10% (w/w) organosolv lignin, determined using ^{13}C NMR spectroscopy at 80 °C.

https://doi.org/10.1021/acs.biomac.3c00047
Biomacromolecules XXXX, XXX, XXX−XXX

xylan ($\Delta\delta \sim 0.43$ ppm), followed by cellulose ($\Delta\delta \sim 0.24$ ppm), and then lignin ($\Delta\delta \sim 0.18$ ppm).

The C10 in acetate ions exhibited an upfield chemical shift in the presence of all three biopolymers. This increase in shielding is often equated to the redistribution of electronic cloud density. However, in the presence of lignin, the shielding of C10 was far higher ($\Delta\delta = -0.25$ ppm) than in the presence of xylan ($\Delta\delta = -0.15$ ppm) or cellulose ($\Delta\delta = -0.12$ ppm), which suggests that there could be direct interactions between C10 and lignin instead of reorganization of electron density (Figure 3). By virtue of hydrogen bonding with C10 atoms, lignin could depict an increase in interactive strength with acetate-ILs.

The absolute total value of chemical shift changes in the presence of cellulose for the four ILs followed the trend of [EMIM][OAc] ~ [AMIM][OAc] > [EMIM][HCOO] > [AMIM][HCOO] (Figure 2). Even though our NMR spectroscopic results suggest that both the [AMIM] and [EMIM] cations are involved in hydrogen bonding with cellulose, the basicity of the corresponding anions appears to ultimately determine the strength of these interactions. When comparing all three biopolymers, lignin exhibited the lowest total absolute value of chemical shift changes, and its interactions with the four ILs followed the order of [AMIM][OAc] > [EMIM][OAc] > [EMIM][HCOO] > [AMIM][HCOO]. Xylan strongly interacted with [AMIM]-[OAc] and followed the trend of [AMIM][OAc] > [AMIM]-[HCOO] ~ [EMIM][OAc] > [EMIM][HCOO]. Overall, these studies reveal that [AMIM][OAc] exhibits the strongest set of interactions with xylan and lignin, which could be attributed to not only its basic anion but also the electro-negative allyl side chains forming bonus hydrogen bonds.

Suprastructural Conformation of Biopolymers in ILs. While NMR data offered information about the atomic level interactions between ILs and plant polymer components, our SAXS studies investigated their suprastructural conformation in specific ILs. Our selection of ILs for SAXS analysis was based on the magnitude of chemical shift changes observed during the NMR studies.

Cellulose Conformation in ILs. Cellulose displayed the largest and least magnitude of total chemical shift changes with [EMIM][OAc] and [AMIM][HCOO], respectively, during NMR analysis. Therefore, SAXS analysis of cellulose was conducted with these two ILs. As shown in Figure 4, the cellulose SAXS profiles are similar for [EMIM][OAc] and [AMIM][HCOO], except for the overall scattering intensity. The observed monotonic linear increase of scattering intensity with decreasing wave vector, Q^{-1}, implies that the cellulose polymer exhibited a rod-like shape in both ILs. The shoulder feature in the high-Q region ($Q > 0.2$ Å^{-1}) represents the average cross-sectional radial dimension of the rod-like particle. Consequently, the SAXS data were fitted to a cylindrical shape. The high flux of synchrotron X-rays was necessary to detect such small cross-sectional dimensions of the rod-shaped particles (~8 Å). The observation of rod-like shape for cellulose is consistent with previous reports.[22,23,34] The concentration of cellulose in [EMIM][OAc] at 2% (w/w) is above the polymer overlap regime (~ 0.8% w/w) but below the level of polymer entanglement (~3% w/w).[22] In this concentration range, cellulose exhibits chain flexibility with a gradual increase in interchain interactions. However, prior to the onset of interchain interactions, cellulose chains are stiff and rod-like[23] (Figure 4) for length scales <70 Å (or $Q > 0.014$ Å^{-1}) due to the rigid β-1,4 bonds connecting individual D-glucose units. And above the entanglement concentration, interchain interactions become dominant, rendering varying degrees of flexibility to cellulose chains.[34] For this study, the chosen concentration of 2% (w/w) of cellulose in IL allowed us to produce sufficient scattering signal while maintaining minimal interchain interactions to allow for the kind of analysis described below.

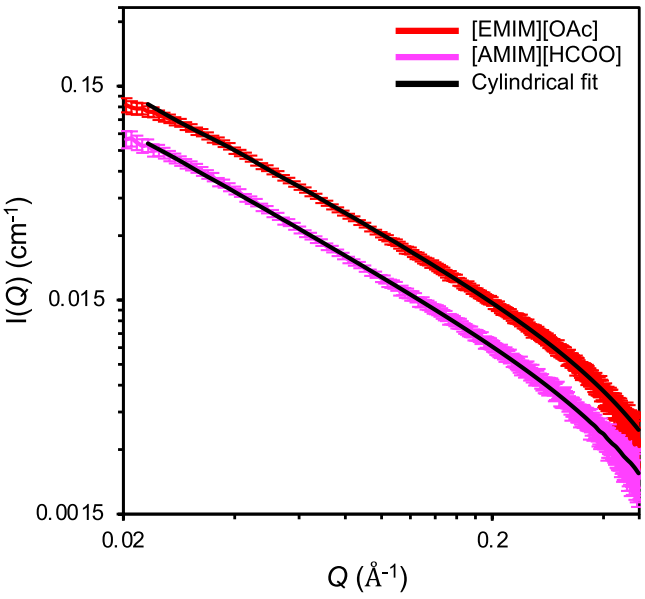

Figure 4. SAXS profiles of 2% (w/w) cellulose in [EMIM][OAc] and [AMIM][HCOO] with a cylindrical shape fit indicated by the solid black lines.

The calculated parameters for cellulose in [EMIM][OAc] and [AMIM][HCOO] are listed in Table 1. The contrast parameter ($\Delta\rho_{exp}$) was fitted after fixing the particle volume fraction (ϕ_p) of cellulose to that of the value calculated from the weights of cellulose and solvent used to prepare the sample. Table 1 shows that the cross-sectional radii of cellulosic cylindrical particles were identical in both ILs, at ~2.9 Å, and the experimental contrast ($\Delta\rho_{exp}$) was higher than the calculated contrast ($\Delta\rho_{calc}$). The main distinction in the fit parameters of cellulose in [AMIM][HCOO] and [EMIM]-[OAc] was in the experimentally measured contrast.

Table 1. Summary of Cylindrical Fit Parameters of SAXS Data for a 2% (w/w) Cellulose Solution in Select ILs

fit parameters	[EMIM][OAc]	[AMIM][HCOO]
[a]volume fraction (ϕ_p)	0.0148	0.0151
mean cylinder radius (Å)	2.89 ± 0.06	2.85 ± 0.06
experimental contrast ($\Delta\rho_{exp}$) (×10^{-6} Å^{-2})	5.14	4.04
[b]calculated contrast ($\Delta\rho_{calc}$) (×10^{-6} Å^{-2})	3.42	3.25
[c]number of anhydroglucose units (AGU) per anion	3	5
[c]number of anhydroglucose units (AGU) per cation	6	13

[a]Calculated from weight percent. [b]Calculated contrast values. [c]Obtained from eq 8.

Raghuwanshi et al. first observed such a difference between the experimental and calculated contrast between ILs and cellulose and developed a method to quantify the stoichiom-

https://doi.org/10.1021/acs.biomac.3c00047
Biomacromolecules XXXX, XXX, XXX−XXX

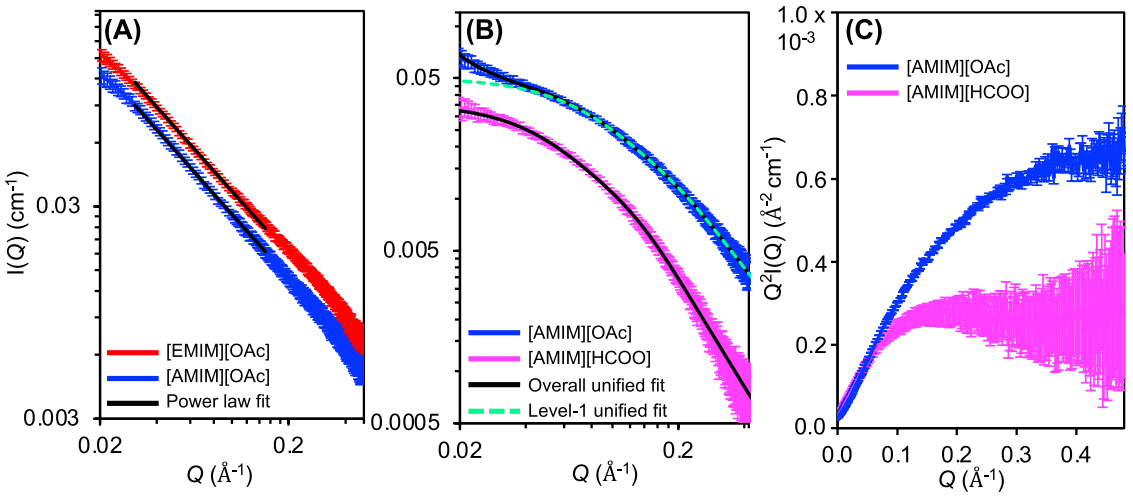

Figure 5. SAXS curves of (A) 2% (w/w) birchwood xylan dissolved in [EMIM][OAc] and [AMIM][OAc]; (B) 2% (w/w) organosolv lignin dissolved in [AMIM][OAc] and [AMIM][HCOO]. The solid black lines are the overall fits. (C) Kratky plots of 2% (w/w) organosolv lignin dissolved in ILs.

etry of closely associated IL-anions and anhydroglucose units (AGUs), the cellulose polymer building block.[24] However, as seen in the ^{13}C NMR results section, both the IL-anions and cations interacted with cellulose; therefore, we modified the formula used by Raghuwanshi et al. to include both possibilities.[24] The expression is given as

$$\text{number of anhydroglucose units per anion(or cation)} = \frac{\left(\frac{(\sum b_i)}{\text{anion(or cation)}} \Big/ \frac{(\sum b_i)}{\text{anhydroglucose}}\right)}{(1 - (\rho_{IL}/\rho_{cellulose}))((\Delta\rho_{exp}/\Delta\rho_{calc}) - 1)} \quad (8)$$

where $(\sum b_i)_{anhydroglucose}$ and $(\sum b_i)_{anion\ (or\ cation)}$ are the scattering lengths of anhydroglucose and the anion (or cation); ρ_{IL} and $\rho_{cellulose}$ are the scattering length densities of the IL and cellulose; and $\Delta\rho_{exp}$ and $\Delta\rho_{calc}$ are the experimental and calculated contrasts, respectively.

Applying this formula to our system and assuming that only anions were involved, we determined that one formate anion binds to 5 AGUs and one acetate anion binds to 3 AGUs (Table 1). Alternatively, the observed increase, in contrast, could be explained by the binding of IL-cations to AGUs. Similar calculations revealed that one [EMIM] cation ion binds to 6 AGUs and one [AMIM] cation binds to 13 AGUs. Irrespective of the assumptions, approximately twice as many [EMIM][OAc] ions were bound to one cellulose molecule than [AMIM][HCOO] ions. Combining both SAXS and ^{13}C NMR results, we can conclude that a higher number of interactions existed between cellulose and [EMIM][OAc] than other ILs. This observation aligns well with previous reports, which concluded, based on vibrational spectroscopy and DFT calculations, that acetate-containing imidazolium-ILs interacted strongly with cellulose when compared to alkyl phosphate-, hydrogen sulfate-, chloride-, tetrafluoroborate-, and hexafluorophosphate-containing ILs.[35,36]

SAXS analysis has been previously used to probe the structure of cellulose in various solvents such as water, acetone, and ethanol.[37,38] A characteristic shoulder has been reported around $Q \sim 0.075-0.1$ Å^{-1} for cellulose dissolved in other aqueous and organic solvents, which is representative of the cross-sectional dimension of a cellulose microfibril (e.g., 30−40 Å).[38] However, in our study, this feature was observed at a higher Q-value, ~0.3 Å^{-1}, which implies that the cross-sectional dimension of the observed cellulosic particle was significantly smaller than the reported dimension of a cellulose microfibril. The measured diameter in both [EMIM][OAc] and [AMIM][HCOO] was approximately 5.8 ± 0.1 Å. This size matches with the calculated cross-sectional diameter of an AGU model structure (6.38 Å),[39] suggesting that these cylindrical particles are elementary cellulose fibrils conforming to a rod-like structure in the tested ILs. The fact that individual cellulose strands were observable indicated that both [EMIM][OAc] and [AMIM][HCOO] penetrated and expanded the cellulose microfibrils and, as a result, replaced the interfibrillar hydrogen bonding with hydrogen bonding between IL-ions and individual elementary cellulose fibrils.

Xylan Conformation in ILs. The largest and least changes in NMR chemical shifts for xylan were observed with [AMIM][OAc] and [EMIM][HCOO], respectively (Figure 3A). However, [EMIM][HCOO] is solid at room temperature, which hindered our ability to extract useful polymer conformational information during our solution-state SAXS experiments. For this reason, the second to last IL, *i.e.*, [EMIM][OAc], was chosen for the structural conformational studies of xylan by SAXS.

SAXS profiles of xylan in the two chosen ILs, [EMIM][OAc] and [AMIM][OAc], showed Q^{-1} pattern identical to that of cellulose, suggesting that xylan also dispersed as individual polymer chains at the molecular level (Figure 5A). This is in contrast to a recent study, where a 5% (w/w) xylan solution formed large aggregates in tetraethylammonium hydroxide, indicating that imidazolium-ILs are superior solvents of xylan.[40] A single power-law function with a fixed exponent of −1, representing a rod-like particle, was fitted to our SAXS data in the Q-range of 0.03−0.15 Å^{-1} (Figure 5A). However, the cross-sectional (shoulder) feature in the high-Q region (Q > 0.2 Å^{-1}) was not clearly observable like that of cellulose. It may be because the cross-sectional dimension of xylan polymer is slightly smaller than cellulose, making it difficult to detect. The scaling factor of the power-law function is related to the volume fraction of the particles (ϕ_p), the volume of a particle (V_p), and contrast between the particle

https://doi.org/10.1021/acs.biomac.3c00047
Biomacromolecules XXXX, XXX, XXX−XXX

and solvent ($\Delta\rho = \rho_{particle} - \rho_{solvent}$), as given by eq 2. The volume fraction of xylan chains was fixed to the value calculated from the weights of xylan and solvent in the sample. The volume of a particle (V_p) was fixed to the calculated diameter of an anhydroxylose unit (AXU). The contrast parameter was the only fit parameter, and the experimentally determined contrast was slightly higher than the calculated contrast values (Table 2). Applying eq 8 with xylan and AXU

Table 2. Summary of Fit Parameters of SAXS Data for a 2% (w/w) Solution of Xylan and Lignin in Select ILs

fit parameters	[EMIM][OAc]	[AMIM][OAc]	[AMIM][HCOO]
Birchwood Xylan			
intensity scalar (cm^{-1} $Å^{-1}$)	0.0027	0.0028	
[a]volume fraction (ϕ)	0.0146	0.0149	
experimental contrast ($\Delta\rho_{exp}$) ($\times 10^{-6}$ $Å^{-2}$)	4.28	4.34	
[b]calculated contrast ($\Delta\rho_{calc}$) ($\times 10^{-6}$ $Å^{-2}$)	3.48	3.59	
[c]number of anhydroxylose unit (AXU) per anion	7	7	
[c]number of anhydroxylose unit (AXU) per cation	13	15	
Organosolv Lignin			
radius of gyration ($R_{g,1}$, Å)		18.2 ± 1.2	27.0 ± 3.0
Guinier scalar (G_1)		0.050	0.071
Porod scalar (B_1)		0.00085	0.00024
power-law exponent (P_1)		1.7 ± 0.1	2.1 ± 0.1

[a]Calculated from weight percent. [b]Calculated from contrast values. [c]Obtained from eq 8.

in place of cellulose and AGU, respectively, the number of AXUs bound to acetate ions was determined to be ~7 in both [EMIM][OAc] and [AMIM][OAc] (Table 2). Furthermore, the number of [EMIM] and [AMIM] cations bound to AXU was calculated to be analogous (13 and 15, respectively). In fact, irrespective of cation or anion, the number of AXUs bound by ILs was similar. However, it is important to note that xylan exhibited the least number of ^{13}C NMR interactions with [EMIM][HCOO]; therefore, there may be an unknown upper threshold in the number of AXUs solvated by an IL-anion. Such a threshold would easily identify noneffective solvents for dissolving plant polysaccharides; from our results, this threshold could be approximately 7 AGUs (or AXUs). Finally, when comparing the fit results of xylan and cellulose systems, the number of AXUs associated with one anion is much higher (7 vs 3) than that of AGUs, suggesting that xylan/anion interaction is weaker than cellulose/anion interaction.

Lignin Conformation in ILs. SAXS profiles of lignin in [AMIM][OAc] and [AMIM][HCOO] are shown in Figure 5B. Unlike cellulose and xylan, lignin formed particles as evidenced by the plateauing of SAXS data in the low-Q region (0.02−0.04 $Å^{-1}$). The two profiles show slight differences, particularly in the position of the shoulder feature, which represents the size of the particle. The slopes in the high-Q region (0.05−0.3 $Å^{-1}$) are better discerned using a Kratky plot, where $I(Q)Q^2$ is plotted as a function of Q (Figure 5C). The gradual manner of leveling in the $I(Q)Q^2$ intensity in the high-Q region for [AMIM][OAc] implies that its slope in the high-Q region was slightly lower than an exponent of 2. As a result, we could conclude that the lignin polymer existed in an expanded (or swollen) state within the larger particle in [AMIM][OAc]. Whereas in the case of [AMIM][HCOO], $I(Q)Q^2$ intensity plateaued in the low-Q region, implying that the lignin polymer conformed as a random Gaussian chain within the larger particle.

The SAXS profiles of lignin in ILs were fitted to a two-level Unified fit function (Figure 5B) with level-1 structural features as the relevant set. A Unified fit, as described in the methods section, basically combines the application of two disjoint functions, namely, Guinier and Porod. The Guinier function was used to obtain R_g and scalar G parameters, while scalar B and exponent P were obtained from the Porod function. Lignin polymer dissolved in [AMIM][OAc] formed particles with $R_{g,1}$ of 18 Å and bulk chain conformations that were swollen and extended ($P_1 \sim 1.7$). This extended conformation of lignin suggests a higher magnitude of lignin-IL interactions than lignin−lignin or IL−IL interactions. On the other hand, lignin formed slightly larger particles in [AMIM][HCOO] with $R_{g,1}$ of 27 Å and exhibited randomly flexible chains with a tendency to entangle ($P_1 \sim 2.1$). A random flexible chain conformation is observed when the polymer−solvent and polymer−polymer interactions are similar in magnitude. However, compared to a swollen/extended conformation of lignin in [AMIM][OAc], a randomly flexible chain indicates a lower magnitude of interactions between lignin and [AMIM][HCOO]. Particles of similar sizes with random coil conformations were previously reported for acetylated softwood and poplar kraft lignins ($R_g \sim 25$ and 16 Å, respectively) dissolved in DMSO.[41] Nonacetylated kraft lignins, on the other hand, formed aggregates in DMSO, proving that DMSO, unlike ILs, was not a good solvent for lignin.[41] This study thus highlights the ability of ILs to solvate lignin polymers.

Furthermore, the molecular weight of lignin in dilute solutions was determined from SAXS data using the Porod invariant approach.[42] The calculated molecular weights of lignin in [AMIM][OAc] and [AMIM][HCOO] were ~4300 and 17 900 g/mol, respectively, assuming that the molecular density of lignin was 1.35 g/cm^3. As mentioned in the Methods section, the M_w of lignin determined using gel permeation chromatography was ~3743 g/mol. This suggests that lignin dispersed as individual molecules in [AMIM][OAc], whereas approximately four polymer molecules associated together in [AMIM][HCOO]. The fact that the molecular weight of lignin was smaller and closer to that of individual molecules (as determined by GPC) implied that [AMIM][OAc] was a better solvent for lignin than [AMIM][HCOO].

CONCLUSIONS

In this study, ^{13}C NMR spectroscopy showed that cellulose, xylan, and lignin polymers interacted differently with select 1,3-dialkylimidazolium ILs. Cellulose exhibited the strongest interactions with [EMIM][OAc], whereas xylan and lignin exhibited significantly higher interactions with [AMIM][OAc]. Significant changes in the ^{13}C chemical shifts of the allyl side chains of [AMIM] in the presence of xylan, and C10 of acetate ion in the presence of lignin accounted for these differences. SAXS results suggested that lignin formed particles with either extended or randomly flexible chain conformation depending on the IL. The higher ^{13}C NMR spectroscopic shifts of lignin in [AMIM][OAc] and its self-avoiding conformation determined using SAXS suggested that [AMIM][OAc] is a superior solvent for lignin. In contrast, SAXS analysis of cellulose and xylan showed similar conformations in all tested ILs, albeit significantly different number of IL-anions or cations being

https://doi.org/10.1021/acs.biomac.3c00047
Biomacromolecules XXXX, XXX, XXX−XXX

bound to anhydroglucose (AGU) and anhydroxylose units (AXU). Twice as many acetates or [EMIM] ions were bound to one AGU as opposed to formate or [AMIM] ions. Moreover, the AGUs exhibited twice as many bonding interactions with acetate anions compared to AXUs. Thus, by combining atomic level interactions and supramolecular conformation of biopolymer/IL systems, 1,3-dialkylimidazolium acetates were shown to exhibit higher set of interactions with all three biopolymers. Finally, parameters developed in this study, namely, the number of IL-ions binding to AGUs/AXUs, could provide critical insights into the design and development of ILs in the future for efficient solubilization of plant polysaccharides.

■ ASSOCIATED CONTENT

Supporting Information

The Supporting Information is available free of charge at https://pubs.acs.org/doi/10.1021/acs.biomac.3c00047.

Moisture content of the neat and biopolymer-IL solutions; annotated ^{13}C NMR spectra of [AMIM][OAc], [AMIM][HCOO], [EMIM][HCOO], and [EMIM][OAc], with and without cellulose, xylan, and lignin; absolute chemical shift changes of cellulose, xylan, and lignin in all tested ILs; and molecular weight, density, and scattering length density of cellulose, xylan, and ILs (PDF)

■ AUTHOR INFORMATION

Corresponding Author

Nicole Labbé − *Center for Renewable Carbon and School of Natural Resources, The University of Tennessee, Knoxville, Tennessee 37996, United States;* orcid.org/0000-0002-2117-4259; Phone: +1 (865) 946-1126; Email: nlabbe@utk.edu

Authors

Aparna Annamraju − *Center for Renewable Carbon and School of Natural Resources, The University of Tennessee, Knoxville, Tennessee 37996, United States*

Kalavathy Rajan − *Center for Renewable Carbon, The University of Tennessee, Knoxville, Tennessee 37996, United States;* orcid.org/0000-0002-1837-1235

Xiaobing Zuo − *X-ray Science Division, Argonne National Laboratory, Lemont, Illinois 60439, United States*

Brian K. Long − *Department of Chemistry, The University of Tennessee, Knoxville, Tennessee 37996, United States*

Sai Venkatesh Pingali − *Center for Structural Molecular Biology and Neutron Scattering Division, Oak Ridge National Laboratory, Oak Ridge, Tennessee 37831, United States;* orcid.org/0000-0001-7961-4176

Thomas J. Elder − *USDA-Forest Service, Southern Research Station, Auburn, Alabama 36849, United States;* orcid.org/0000-0003-3909-2152

Complete contact information is available at: https://pubs.acs.org/10.1021/acs.biomac.3c00047

Author Contributions

The manuscript was written through contributions of all authors. All authors have given approval to the final version of the manuscript.

Funding

This work was supported by the Research Council of Norway (BioMim project) and the U.S. Forest Service, Southern Research Station (Award #19-JV-594 1130131-026). Partial funding was also obtained from the U.S. DOE Office of Science, under the Biological and Environmental Research Program (FWP ERKP752−Genomic Science Program, and FWP ERKP291−The Center for Structural Molecular Biology). This research used resources of the Advanced Photon Source; a U.S. Department of Energy (DOE) Office of Science user facility operated for the DOE Office of Science by Argonne National Laboratory under Contract No. DE-AC02-06CH11357. Oak Ridge National Laboratory is managed by UT-Battelle, LLC, for the U.S. Department of Energy under Contract DE-AC05-00OR22725. This manuscript has been coauthored by UT-Battelle, LLC, under Contract No. DE-AC05-00OR22725 with the U.S. Department of Energy. The United States Government retains and the publisher, by accepting the article for publication, acknowledges that the United States Government retains a nonexclusive, paid-up, irrevocable, worldwide license to publish or reproduce the published form of this manuscript, or allow others to do so, for United States Government purposes. The Department of Energy will provide public access to these results of federally sponsored research in accordance with the DOE Public Access Plan (http://energy.gov/downloads/doe-public-access-plan).

Notes

The authors declare no competing financial interest.

■ ACKNOWLEDGMENTS

The authors thank Dr. Carlos A. Steren from the Department of Chemistry, the University of Tennessee Knoxville, for assisting with the NMR experiments. The authors also thank Dr. Byeongdu Lee at Advanced Photo Source, Argonne National Laboratory, for useful discussions on SAXS data analysis. Finally, the authors would like to thank Dr. Yachin Cohen from the Department of Chemical Engineering, Technion Israel Institute of Technology, Haifa, for email correspondence on biopolymer ion binding calculations.

■ REFERENCES

(1) McCann, M. C.; Carpita, N. C. Biomass recalcitrance: A multi-scale, multi-factor, and conversion-specific property. *J. Exp. Bot.* **2015**, *66*, 4109−4118.

(2) Karimi, K.; Shafiei, M.; Kumar, R. Progress in Physical and Chemical Pretreatment of Lignocellulosic Biomass. In *Biofuel Technologies: Recent Developments*, Gupta, V. K.; Tuohy, M. G., Eds.; Springer Inc.: Berlin, Heidelberg, 2013; pp 53−96.

(3) Wang, H.; Pu, Y.; Ragauskas, A.; Yang, B. From lignin to valuable products−strategies, challenges, and prospects. *Bioresour. Technol.* **2019**, *271*, 449−461.

(4) Huang, L.-Z.; Ma, M.-G.; Ji, X.-X.; Choi, S.-E.; Si, C. Recent developments and applications of hemicellulose from wheat straw: A review. *Front. Bioeng. Biotechnol.* **2021**, *9*, No. 690073.

(5) Ma, C.; Kim, T.-H.; Liu, K.; Ma, M.-G.; Choi, S.-E.; Si, C. Multifunctional lignin-based composite materials for emerging applications. *Front. Bioeng. Biotechnol.* **2021**, *9*, No. 708976.

(6) Rosenau, T.; Potthast, A.; Adorjan, I.; Hofinger, A.; Sixta, H.; Firgo, H.; Kosma, P. Cellulose solutions in N-methylmorpholine-N-oxide (NMMO) − degradation processes and stabilizers. *Cellulose* **2002**, *9*, 283−291.

(7) Wikandari, R.; Millati, R.; Taherzadeh, M. J. Pretreatment of Lignocelluloses with Solvent N-Methylmorpholine N-oxide. In *Biomass Fractionation Technologies for A Lignocellulosic Feedstock*

Based Biorefinery, Mussatto, S. I., Ed.; Elsevier: Amsterdam, 2016; pp 255−280.
(8) Miki, K.; Kamitakahara, H.; Yoshinaga, A.; Tobimatsu, Y.; Takano, T. Methylation-triggered fractionation of lignocellulosic biomass to afford cellulose-, hemicellulose-, and lignin-based functional polymers via click chemistry. *Green Chem.* **2020**, *22*, 2909−2928.
(9) Ghosh, A.; Kim, K.; Rajan, K.; Bowland, C. C.; Gurram, R. N.; Montgomery, R. W.; Manesh, A.; Labbé, N.; Naskar, A. K. Butanol-based organosolv lignin and reactive modification of poly(ethylene-glycidyl methacrylate). *Ind. Eng. Chem. Res.* **2019**, *58*, 20300−20308.
(10) Brandt, A.; Gräsvik, J.; Halletta, J. P.; Welton, T. Deconstruction of lignocellulosic biomass with ionic liquids. *Green Chem.* **2013**, *15*, 550−583.
(11) Swatloski, R. P.; Spear, S. K.; Holbrey, J. D.; Rogers, R. D. Dissolution of cellose with ionic liquids. *J. Am. Chem. Soc.* **2002**, *124*, 4974−4975.
(12) Hart, W. E. S.; Harper, J. B.; Aldous, L. The effect of changing the components of an ionic liquid upon the solubility of lignin. *Green Chem.* **2015**, *17*, 214−218.
(13) Yuan, L.; Peng, H.; Hu, L.; Yu, R.; Peng, W.; Ruan, R.; Xia, Q.; Zhang, Y.; Liu, A. Dissolution of bamboo hemicellulose in 1-butyl-3-methylimidazolium halide-based ionic liquids. *BioRes.* **2019**, *14*, 2097−2112.
(14) Remsing, R. C.; Swatloski, R. P.; Rogers, R. D.; Moyna, G. Mechanism of cellulose dissolution in the ionic liquid 1-n-butyl-3-methylimidazolium chloride: A ^{13}C and $^{35/37}Cl$ NMR relaxation study on model systems. *Chem. Commun.* **2006**, *12*, 1271−1273.
(15) Zhang, J.; Zhang, H.; Wu, J.; Zhang, J.; Hea, J.; Xiang, J. NMR spectroscopic studies of cellobiose solvation in EmimAc aimed to understand the dissolution mechanism of cellulose in ionic liquids. *Phys. Chem. Chem. Phys.* **2010**, *12*, 1941−1947.
(16) Zhang, J.; Xu, L.; Yu, J.; Wu, J.; Zhang, X.; He, J.; Zhang, J. Understanding cellulose dissolution: Effect of the cation and anion structure of ionic liquids on the solubility of cellulose. *Sci. China Chem.* **2016**, *59*, 1421−1429.
(17) Zhang, Y.; Xu, A.; Lu, B.; Li, Z.; Wang, J. Dissolution of cellulose in 1-allyl-3-methylimizodalium carboxylates at room temperature: A structure−property relationship study. *Carbohydr. Polym.* **2015**, *117*, 666−672.
(18) Hu, L.; Peng, H.; Zhang, Y.; Xia, Q.; He, H.; Ruan, R.; Liu, Y.; Liu, A. Insight into the interaction between arabinoxylan and imidazolium acetate-based ionic liquids. *Carbohydr. Polym.* **2020**, *231*, No. 115699.
(19) Payal, R. S.; Bharath, R.; Periyasamy, G.; Balasubramanian, S. Density functional theory investigations on the structure and dissolution mechanisms for cellobiose and xylan in an ionic liquid: Gas phase and cluster calculations. *J. Phys. Chem. B* **2012**, *116*, 833−840.
(20) Janesko, B. G. Modeling interactions between lignocellulose and ionic liquids using DFT-D. *Phys. Chem. Chem. Phys.* **2011**, *13*, 11393−11401.
(21) Singh, S. K.; Dhepe, P. L. Ionic liquids catalyzed lignin liquefaction: Mechanistic studies using TPO-MS, FT-IR, RAMAN and 1D, 2D-HSQC/NOSEY NMR. *Green Chem.* **2016**, *18*, 4098−4108.
(22) Napso, S.; Rein, D. M.; Khalfin, R.; Cohen, Y. Semidilute solution structure of cellulose in an ionic liquid and its mixture with a polar organic co-solvent studied by small-angle X-ray scattering. *J. Polym. Sci. B Polym. Phys.* **2017**, *55*, 888−894.
(23) Jiang, X.; Kitamura, S.; Sato, T.; Terao, K. Chain dimensions and stiffness of cellulosic and amylosic chains in an ionic liquid: Cellulose, amylose, and an amylose carbamate in BmimCl. *Macromolecules* **2017**, *50*, 3979−3984.
(24) Raghuwanshi, V. S.; Cohen, Y.; Garnier, G.; Garvey, C. J.; Russell, R. A.; Darwish, T.; Garnier, G. Cellulose dissolution in ionic liquid: Ion binding revealed by neutron scattering. *Macromolecules* **2018**, *51*, 7649−7655.
(25) Hesse-Ertelt, S.; Heinze, T.; Kosan, B.; Schwikal, K.; Meister, F. Solvent effects on the NMR chemical shifts of imidazolium-based ionic liquids and cellulose therein. *Macromol. Symp.* **2010**, *294*, 75−89.
(26) Fukaya, Y.; Sugimoto, A.; Ohno, H. Superior solubility of polysaccharides in low viscosity, polar, and halogen-free 1,3-dialkylimidazolium formates. *Biomacromolecules* **2006**, *7*, 3295−3297.
(27) Tao, J.; Hosseinaei, O.; Delbeck, L.; Kim, P.; Harper, D. P.; Bozell, J. J.; Rials, T. G.; Labbé, N. Effects of organosolv fractionation time on thermal and chemical properties of lignins. *RSC Adv.* **2016**, *6*, 79228−79235.
(28) Zhao, Y.; Liu, X.; Wang, J.; Zhang, S. Insight into the cosolvent effect of cellulose dissolution in imidazolium-based ionic liquid systems. *J. Phys. Chem. B* **2013**, *117*, 9042−9049.
(29) Zhang, F.; Ilavsky, J.; Long, G. G.; Quintana, J. P. G.; Allen, A. J.; Jemian, P. R. Glassy Carbon as an absolute intensity calibration standard for small-angle scattering. *Metall. Mater. Trans. A* **2010**, *41*, 1151−1158.
(30) Ilavsky, J.; Jemian, P. R. Irena: Tool suite for modeling and analysis of small angle scattering. *J. Appl. Crystallogr.* **2009**, *42*, 347−353.
(31) Beaucage, G. Small-angle scattering from polymeric mass fractals of arbitrary mass-fractal dimension. *J. Appl. Crystallogr.* **1996**, *29*, 134−146.
(32) Chen, Y.; Li, S.; Xue, Z.; Hao, M.; Mu, T. Quantifying the hydrogen-bonding interaction between cation and anion of pure [EMIM][Ac] and evidencing the ion pairs existence in its extremely diluted water solution: Via ^{13}C, ^{1}H, ^{15}N and 2D NMR. *J. Mol. Struct.* **2015**, *1079*, 120−129.
(33) Basa, M. *Ionic Liquids: Solvation Characteristics and Cellulose Dissolution*; University of Toledo: Toledo, OH, 2010; p 200.
(34) Hirosawa, K.; Fujii, K.; Hashimoto, K.; Shibayama, M. Solvated structure of cellulose in a phosphonate-based ionic liquid. *Macromolecules* **2017**, *50*, 6509−6517.
(35) Guo, J.; Zhang, D.; Duan, C.; Liu, C. Probing anion-cellulose interactions in imidazolium-based room temperature ionic liquids: A density functional study. *Carbohydr. Res.* **2010**, *345*, 2201−2205.
(36) Gao, Y.; Zhang, L.; Wang, Y.; Li, H. Probing electron density of H-bonding between cation-anion of imidazolium-based ionic liquids with different anions by vibrational spectroscopy. *J. Phys. Chem. B* **2010**, *114*, 2828−2833.
(37) Leppänen, K.; Pirkkalainen, K.; Penttilä, P.; Sievänen, J.; Kotelnikova, N.; Serimaa, R. Small-angle X-ray scattering study on the structure of microcrystalline and nanofibrillated cellulose. *J. Phys. Conf. Ser.* **2010**, *247*, No. 012030.
(38) Pingali, S. V.; Urban, V. S.; Heller, W. T.; McGaughey, J.; O'Neill, H. M.; Foston, M.; Myles, D. A.; Ragauskas, A. J.; Evans, B. R. SANS study of cellulose extracted from switchgrass. *Acta Crystallogr. D Biol. Crystallogr.* **2010**, *66*, 1189−1193.
(39) Nishiyama, Y.; Langan, P.; Chanzy, H. Crystal structure and hydrogen-bonding system in cellulose Iβ from synchrotron X-ray and neutron fiber diffraction. *J. Am. Chem. Soc.* **2002**, *124*, 9074−9082.
(40) Liu, Q.; Tian, R.; Lv, Z.; Wu, Y.; Lv, B.; Hao, X.; Xue, Z.; Peng, F. Rapid, selective, and room temperature dissolution of crystalline xylan by a hydrotrope. *Carbohydr. Polym.* **2023**, *300*, No. 120245.
(41) Zhao, W.; Xiao, L.-P.; Song, G.; Sun, R.-C.; He, L.; Singh, S.; Simmons, B. A.; Cheng, G. From lignin subunits to aggregates: Insights into lignin solubilization. *Green Chem.* **2017**, *19*, 3272−3281.
(42) Piiadov, V.; Ares de Araújo, E.; Oliveira Neto, M.; Craievich, A. F.; Polikarpov, I. SAXSMoW 2.0: Online calculator of the molecular weight of proteins in dilute solution from experimental SAXS data measured on a relative scale. *Protein Sci.* **2019**, *28*, 454−463.

https://doi.org/10.1021/acs.biomac.3c00047
Biomacromolecules XXXX, XXX, XXX−XXX